J Mol Model (2012) 18:2301–2310
DOI 10.1007/s00894-011-1240-z

ORIGINAL PAPER

Exploration of the valproic acid binding site on histone deacetylase 8 using docking and molecular dynamic simulations

Jorge Antonio Bermúdez-Lugo · Oscar Perez-Gonzalez · Martha Cecilia Rosales-Hernández · Ian Ilizaliturri-Flores · José Trujillo-Ferrara · Jose Correa-Basurto

Received: 7 March 2011 / Accepted: 9 September 2011 / Published online: 4 October 2011

Abstract Epigenetic therapy is an important focus of research for drug development in the treatment of cancer. Valproic acid (VPA) is an HDAC inhibitor that has been evaluated in clinical studies. Despite its success in treating cancer, the mechanism of inhibition of VPA in HDAC is unknown. To this end, we have used docking and molecular dynamic simulations to investigate VPA binding to HDAC, employing both native and rebuilt 3-D structures. The results showed that VPA, via its carboxyl group, coordinates the Zn atom and other local residues (H141-142 and Y360) located at the catalytic site (CS) of HDAC. This causes electrostatic and hydrogen bonding interactions while having little interaction with the hydrophobic side chains, resulting in a low affinity. However, after several docking studies on different native HDAC 3-D structures and after using several snapshots from MD simulations, it became apparent that VPA bound with highest affinity at a site located at the acetyl-releasing channel, termed the hydrophobic active site channel (HASC). The affinity of VPA for HASC was due to its highly hydrophobic properties that allow VPA to take part in van der Waals interactions with Y18, I19, Y20, V25, R37, A38, V41, H42, I135 and W137, while VPA's carboxylate group has several hydrogen bonding interactions with the backbones of S138, I19, N136 and W137. MD simulations showed that the HASC door continuously opened and closed, which affected the affinity of VPA to the HASC, but the affinity toward the HASC was consistently higher than that obtained for the CS, suggesting that the HASC could be involved in the mechanism of inhibition.

Keywords Anticancer drugs · Catalytic site · Hydrophobic active site channel · Theoretical studies

J. A. Bermúdez-Lugo · M. C. Rosales-Hernández · I. Ilizaliturri-Flores · J. Trujillo-Ferrara · J. Correa-Basurto (✉)
Laboratorio de Modelado Molecular y Bioinformatica,
Sección de Estudios de Posgrado e Investigacion,
Escuela Superior de Medicina, Instituto Politécnico Nacional,
Plan de San Luis y Díaz Mirón,
11340, Mexico City, Mexico
e-mail: jcorreab@ipn.mx

O. Perez-Gonzalez
Experimental Oncology Laboratory,
National Institute of Pediatrics,
Mexico City, Mexico

Introduction

The epigenetic processes controlled by histone acetyltransferase (HAT) and histone deacetylase (HDAC) have been widely studied, as these proteins represent emerging targets for functional modification in certain diseases, such as cancer [1] and HIV [2].

HDAC belongs to a family of 18 proteins that catalyzes the deacetylation of acetylated ε-amino lysines in histone tails. The proteins are divided into four groups based on their homology domain, their cofactors, and their ability to shuttle between the nucleus and the cytoplasm. HDAC isoforms 1, 2, 3 and 8 belong to class I, while isoforms 4, 5, 6, 7, 9 and 10 belong to class II. The class I isoforms are usually located in the nucleus and require a zinc ion (Zn) for activity, while the class II isoforms can be located in either the nucleus or the cytoplasm, depending on the cell's metabolic needs. Class IV contains only one isoform, HDAC11, which significantly differs in its domain composition compared to other HDAC isoforms. It is believed that HDAC11 diverged earlier in evolution than the other isoforms. Finally, class III consists

of isoforms that require NAD(+) as a cofactor, and they are commonly known as sirtuins [3].

Several HDAC inhibitors (HDACIs) have exhibited anticancer activity and are currently regarded as a new approach to cancer treatment. Their activity has been evaluated from the altered patterns of gene expression observed in neoplastic cells from aberrant HDAC recruitment [4]. When cancer cells are treated with HDACIs, growth arrest, apoptosis or differentiation of the cells is often observed [5–7].

HDACIs are classified according to their chemical structure. Most are nonselective between HDAC isoforms from class I and II [8]. Valproic acid (VPA) is a well-known anti-epileptic and mood-stabilizing drug, and it is also an HDACI [9]. VPA causes growth arrest and induces differentiation of transformed cell cultures by inhibiting multiple class I and II HDACs (but not isoforms 6 and 10) [8, 10]. There is evidence that VPA induces the hyperacetylation of core H3 and H4 with low potency (Ki≈mM), which causes differentiation in hematopoietic cell lines in a p21-dependent manner [10]. VPA has been used for therapy in prostate cancer cells and in vivo models from prostate cancer xenografts. Acute administration of VPA has been shown to produce net histone H3 acetylation as well as up-regulation of p21, androgen receptors, and prostate specific androgen (PSA). The chronic treatment, however, led to a decrease in the net proliferation rate due to an increased expression of caspases 2 and 3 [11].

Due to the well-known antitumor activity associated with VPA after decades of usage as a relatively well-tolerated drug, many phase I and II studies have reported that its utility in treating different types of tumors is a result of HDAC inhibition [12]. A phase II clinical trial of the use of VPA to treat castration-resistant prostate cancer concluded that the PSA (used to monitor disease evolution) correlated inversely with VPA levels, even though VPA treatments produced many adverse effects [13]. Mora-Garcia and coworkers demonstrated the advantages of using VPA in combination with hydralazine (a non-nucleoside DNA methylation inhibitor) as an adjuvant for immune intervention in cervical cancer patients. The global effect from a combination of these two epigenetic modifiers was the cell expression of immune molecules that were absent prior to treatment [14]. Moreover, another study demonstrated that the combination of hydralazine and VPA caused potent growth inhibition for certain cell cancer lines [15]. There are sufficient experimental data to demonstrate the inhibitory activity of VPA with regard to HDAC, but these data have not been investigated in detail at the molecular level.

The carboxyl group of VPA interacts with the Zn atom at the HDAC binding site electrostatically, thereby providing VPA recognition [16]. Exploring the extra ligand-binding pocket, or orthostatic site, is straightforward using docking [17] and molecular dynamic (MD) simulations [18]. These simulations are generally corroborated by experimental methods [19]. Therefore, we have employed docking and MD simulations to understand the binding mode of VPA onto HDAC8 at the atomic level by employing a set of 14 native 3-D structures retrieved from the Protein Data Bank (PDB) and using several snapshots retrieved from MD simulations captured every 0.5 ns over a time span of 9 ns.

Materials and methods

General procedure

To use all of the 3-D structures of HDAC attained from the experimental methods, a search of the PDB was performed, which found 14 structures that belonged to isoform 8 (PDB codes: 1T64 [20], 1T67 [20], 1T69 [20], 1VKG [20], 1W22 [21], 2V5W [22], 2V5X [22], 3EW8 [22], 3EWF [23], 3EZP [23], 3EZT [23], 3F0R [23], 3F06 [23], 3F07 [23]). A multiple alignment was carried out with clustalW2 [24], and the results were edited and analyzed with Jalview [25] to find similarities and differences in the sequences among the reported 3-D structures. The 3-D structures were used for docking simulations as the native structures (initial coordinates). Then, the missing residues at the N- and C-terminals and in the middle of the protein sequence were built using MODELLER [26], and a minimization of the energy of the whole protein was performed on both the native and fulfilled structures.

Docking protocol

VPA was drawn with the Isisdraw program [27], and its geometry was optimized using Hyperchem (Version 6.0, Hypercube, USA, http://www.hyper.com) [28] at the molecular mechanic level. Afterward, a Gaussian program [29] was used to complete the optimization to AM1 and then to B3LYP (6-31G* *d,p*) basis sets. Water molecules and other ligands were removed from HDAC8 PDB structures while the Zn atom was retained. AutoDockTools was used to prepare the blind docking study with a grid box of 126×126×126 Å (distance between two grid points was set to 0.375 Å), centering the grid box on the protein, which was rigid. We used a Lamarckian genetic algorithm to perform the search with an initial population of 100 random individuals, and 1.0×10^7 iterations were run with the AutoDock 4.0.1 [30] program. The results were analyzed with AutoDockTools and the Accelrys Discovery Studio Visualizer. To validate the docking procedure, the protein was re-docked with the co-crystallized ligand using a PDB structure 1F07, which

has APHA as ligand. The energy in the docking studies was calculated as a function of the following five terms:

$$\Delta G = \Delta G_{vfW} \sum_{i,j} \left(\frac{A_{i,j}}{r_{ij}^{12}} - \frac{B_{ij}}{r_{ij}^{6}} \right) + \Delta G_{hbond} \sum_{ij} E(t) \left(\frac{C_{ij}}{r_{ij}^{12}} - \frac{D_{ij}}{r_{ij}^{10}} \right) + \Delta G_{elec} \sum_{ij} \frac{q_i q_j}{\in (r_{ij}) r_{ij}} + \Delta G_{tor} N_{tor} + \Delta G_{sol} \sum_{ij} (S_i V_j + S_j V_i) e^{\left(\frac{-r_{ij}^2}{2\sigma^2} \right)} \quad (1)$$

where the five ΔG terms on the right-hand side are empirically determined coefficients using linear regression analysis from a set of protein-ligand complexes with known binding constants [30].

Molecular dynamics protocol

The input protein coordinates were taken from the structure with PDB code 3F07 because it had the fewest number of missing residues and it did not contain any mutations. The MD simulations were carried out using NAMD2.6 [31] with a CHARMM27 force field [32]. The protein was cleaned of water molecules and the ligand APHA, and the missing loops were constructed with MODELLER [26]. Hydrogen

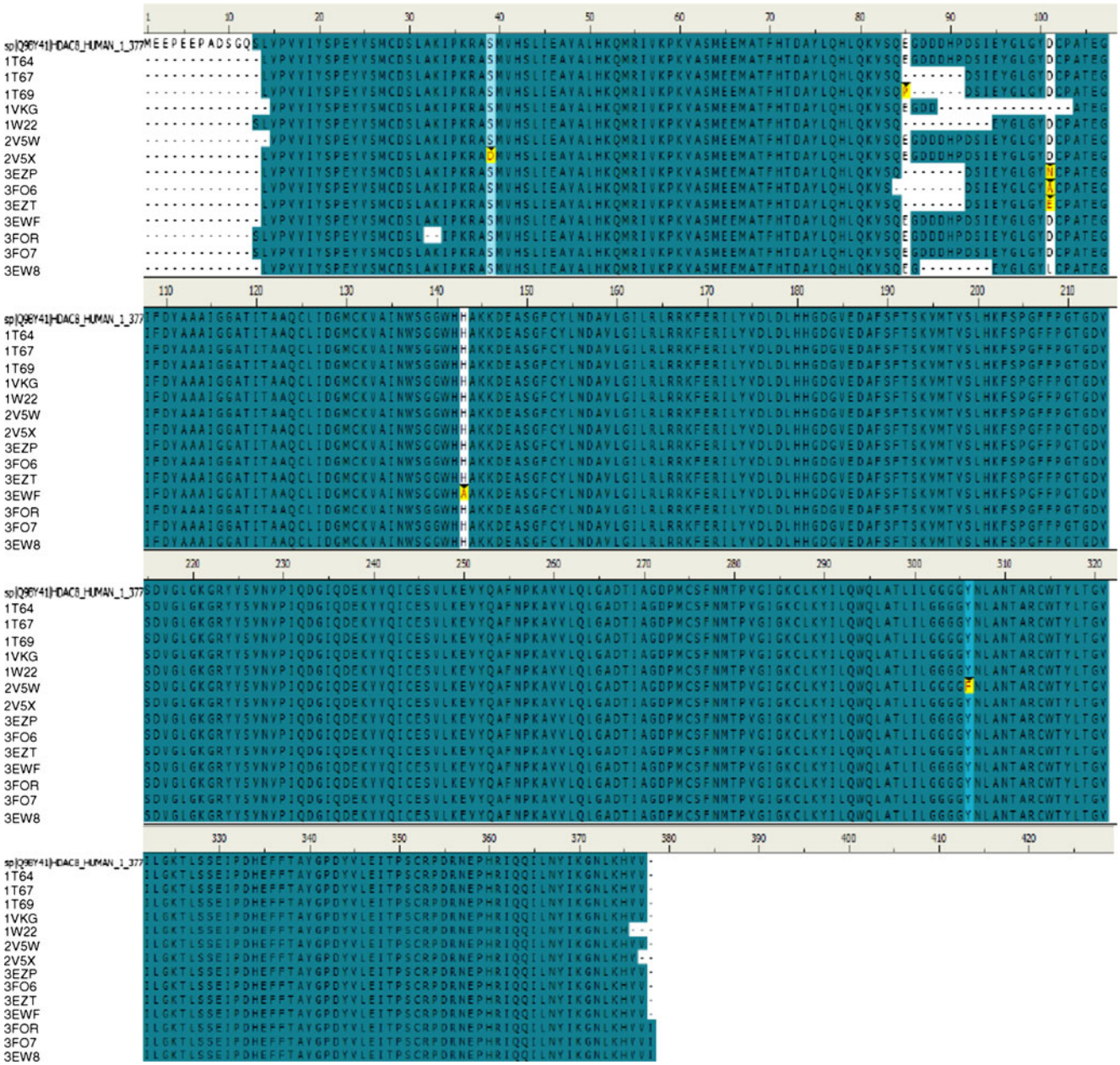

Fig. 1 Sequence alignments of the HDAC8 crystallized structures. The HDAC sequence differences. The missing residues and mutations are in yellow

atoms were added with the psfgen command within the VMD program [33], and the structure was minimized using the steepest descent algorithm for 2000 steps using a CHARMM27 force field [32] and processed with NAMD2. The resultant structure was immersed in a TIP3 water box, and the charge was neutralized. The particle-mesh Ewald method [34] and periodic boundary conditions were applied to complete the electrostatic calculations. We used Nose-Hoover Langevin piston pressure control and maintained temperature at 310 K [35]. The SHAKE [36] method was used to provide an integration time step of 2 fs while keeping all bonds to the hydrogen atoms rigid. The equilibration protocol involved 1500 minimization steps followed by 30 ps of MD at 0 K of water and ions while freezing the entire protein. Once the minimization of the whole system was achieved, the temperature was increased from 10 to 310 K over 30 ps to ensure that it could continue to modify its volume with 30 ps of NTP dynamics [35]. As a final step, the NTV dynamics continued for 9.5 ns. The trajectory of the system was stored at every 1 ps, and the simulations were analyzed by capturing several snapshots every 0.5 ns. All snapshots and the RMSD calculation were obtained with carma program [37]. Each one of these conformations was submitted to a docking simulation with VPA.

Results and discussion

In this study, we combined docking and MD simulations to explore the affinity and recognition between VPA and the HDAC isoform 8. The first step was to retrieve all 14 HDAC8 3-D structures from the PDB, which were then subjected to multiple sequence alignment studies. These studies showed variations in the sequences, as are depicted in Fig. 1. Afterward, all HDAC8 3-D structures were submitted to docking simulations using VPA as the ligand, which was validated with RMSD values between the docked VPA and co-crystallized ligands of less than 2 Å (data not shown). The free energy (ΔG) and Kd values resulting from the interaction between VPA and each HDAC8 tested are listed in Table 1. Table 1 shows two values belonging to two binding sites. One of these is the catalytic site (CS) where the Zn atom is located, which has been the principal target for ligand design [38]. However, in the CS, there are few structural differences between all the HDAC families that cause ligands to act as pan-inhibitors due to their nonspecific inhibition. The principal pan-inhibitors are suberoylanilide hydroxamic acid (SAHA) and trycostatine (TSA) [39]. From the ΔG values that could be influenced from the X-ray protein structure resolution (Table 1), we showed that there was no correlation between the resolution and ΔG values in either the native PDB or the minimized 3-D structures.

The great majority of the HDACIs interact with the CS by making several hydrogen bonds with the carboxyl or hydroxamic acids, and some compounds that possess an aromatic moiety act selectively. Tubacin, which is structurally related to SAHA [40], is an example of this. There is evidence that suggests that the VPA carboxyl moiety interacts with the CS by forming hydrogen bonds and

Table 1 Free energy values (ΔG, kcal mol^{-1}) of interactions between VPA and HDAC8 obtained by docking simulations

HDAC8 structure condition		Native		Docking (loop added)		Minimization		Minimization (loop added)	
Active sites of HDAC8		CS	HASC	CS	HASC	CS	HASC	CS	HASC
PDB code	X-ray resolution (Å)	ΔG	ΔG	ΔG	ΔG	ΔG	ΔG	ΔG	ΔG
1T64	1.9	−6.24	−6.33	−6.42	−7.17	−4.25	−5.63	−4.72	−5.56
1T67	2.31	−4.56	−6.63	−6.16	−6.88	−4.1	−5.8	−4.58	−5.67
1T69	2.91	−4.96	−7.17	−6.57	−7.19	−4.25	−6.47	−4.91	−5.34
1VKG	2.2	−5.25	−6.82	−5.36	−6.98	−4.36	−6.81	—	—
1W22	2.5	−6.72	−7.33	−6.48	−7.36	−4.59	−5.93	−4.75	−6.54
2V5W	2	−5.88	−6.88	−5.94	−7.21	−4.51	−6.23	−4.65	−5.5
2V5X	2.25	−4.8	−6.77	−6.18	−6.95	−4.43	−6.59	−4.87	−5.72
3EW8	1.8	−5.98	−6.87	−6.17	−6.76	−5.24	−6.72	−4.85	−6.68
3EWF	2.5	−5.98	−6.22	−5.9	−6.69	−4.69	−6.75	−5.22	−6.67
3EZP	2.65	−6.29	−6.77	−5.95	−6.49	−5.08	−6.7	−4.61	−6.56
3EZT	2.85	−6.07	−7.01	−5.77	−6.91	−4.98	−6.55	−4.82	−6.52
3F0R	2.54	−5.94	−5.75	−5.84	−6.58	−4.37	−6.22	−4.88	−5.82
3F06	2.55	−6.31	−6.91	−6.08	−6.96	−5.09	−6.62	−4.94	−6.76
3F07	3.3	−6.25	−7.08	−6.23	−7.01	−4.73	−6.78	−4.67	−5.72

electrostatic interactions between specific side chain residues (H142-143 and Y306) and the Zn atom, respectively. These implications are in agreement with results from docking studies [16]. However, there is no evidence that the VPA hydrophobic chain interactions at the CS are due to neighboring aromatic residues, which explains the high affinity of other known HDACIs. For this reason, we focused our study on applying MD simulations to several HDAC8 structures retrieved from the PDB to explore the VPA binding to the sampled 3-D structures.

The docking strategy was used to explore the entire protein using a blind docking procedure to allow VPA to reach all potential binding pockets and to accommodate those with the greatest affinity. Table 1 shows the ΔG and affinity values of VPA, which showed the highest affinities for the hydrophobic active site channel (HASC), where some miscellaneous HDACIs have been shown to bind [41]. It should be noted that the ligands reported to bind to the HASC possess highly hydrophobic chains, such as the cyclostellettamines. The HASC is located in a hydrophobic channel where the acetate is believed to be released after HDAC catalyzes the histone deacetylation. Table 1 also contains all of the 3-D structures investigated using VPA as the ligand, and VPA exhibited stronger affinity to the HASC than to the CS in all structures except for PDB 3F0R. This difference in affinity could be a result of the 3F0R missing two residues (A32 and K33) compared to the other sequences, as illustrated in Fig. 1.

The higher affinity of VPA for the HASC than the CS was shown in all 3-D structures tested (native [except 3F0R], rebuilt and minimized after rebuilt), suggesting that the HASC could be the VPA binding site. This would explain its structural differences compared to other HDACIs, which are typically larger and can form several hydrogen bonds as acceptors or donors. Also, their aromatic moieties make Π-Π interactions with the neighboring aromatic residues near the CS [38]. In contrast, VPA is a small ligand and has a high lipid partition coefficient due to its two hydrocarbon chains [42]. Consequently, these physicochemical properties could explain VPA's high affinity for the HASC located in the acetyl release channel in all HDAC8 3-D structures tested. This acetyl release channel has been verified experimentally [41] and was characterized using X-ray methods by Vaninni and Wang [21, 43]. The acetyl release channel connects the CS, HASC, and the "back door," which is regulated by conformational changes of HDAC8 -helixes 1 and 2. Also, this tunnel is an important area because it is where the free acetate is released after histone deacetylation is carried out at the CS. The VPA docking with native and re-built 3-D HDACs resulted in ΔG and Kd values with higher affinities at the HASC than the CS (see Table 1). To explain these results, we examined the 3-D structural details to help explain these differences. Shown in Fig. 2 are docking results from the native 3-D HDAC structure of PDB 3F0R. These docking results show that the carboxyl group of the VPA binds to the CS by coordination with both the Zn ion and hydrogen bond acceptors, such as Y306, H142 and H143 side chains, as has been reported for an HDAC homologue and VPA complexes [16]. However, Fig. 2b illustrates that VPA hydrophobic chains do not interact because only polar residues, such as H142 and H143 and Y306, are in close proximity. The arrangement resulting in the highest affinity between the HASC and VPA was due to the VPA carboxyl moiety making several hydrogen bonding interactions with the side chains of Y24 and S138 as well as with the backbone amides from I19, S138, and W137. The VPA side chain moieties also formed hydrophobic interactions with the aromatic cluster of Y18, Y20 and W37 as well as with the side chains of V25, I19 and I135.

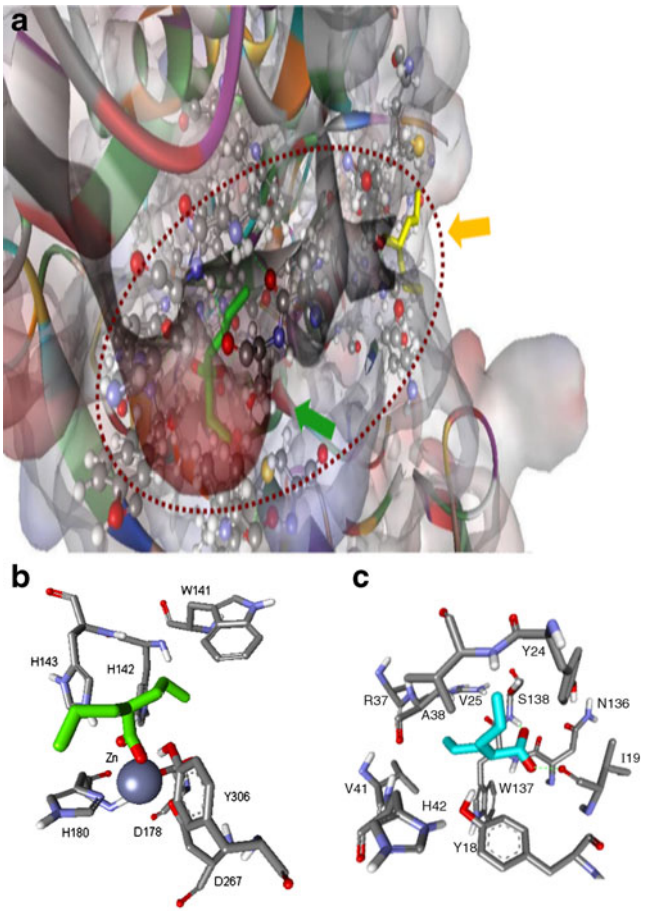

Fig. 2 Interaction of VPA with HDAC8. (**a**) Docked VPA (yellow) blocking the catalytic site (yellow arrow) and VPA (green) in the acetate release channel (green arrow). (**b**) VPA interacting with residues of the catalytic site (left) and the acetate release channel (right). (**c**) Close-up of the stabilization of VPA with the acetate release channel residues

The ΔG values from Table 1 that changed significantly in some HDAC 3-D structures could be explained by an alignment study, as shown in Fig. 1. This figure demonstrates that there are some mutations, that could be relevant for ligand recognitions and protein structure, which include E85P (1T69), S39D (2B5X), D101N (3EZP), D101A (3F06), D101E (3EZT), D101L (3EW8), H143A (3EHF), Y306F (2V5W), N357H (3EZP, 3F06, 3EZT, 3F0R, 3FO7, 3EWS), and H357A (3EWF). Figure 1 also shows that other structures possessed deletions, including 85–91 (1T67, 3EZP, 3EZT), 86–91 (1T69), 89–102 (1VKG), 85–94 (1W22), 84–91 (3F06), 83–93 (3EW8), and 32–33 (3F0R). It is clear that these mutations or deletions altered the binding between VPA and HDAC. The 2V5W structure contained a mutation at Y306F, but the affinity was not modified. This is because both of those amino acids are aromatic and also because residue 306 does not appear to be involved in VPA recognition due to the proximity of the VPA hydrophobic side chain in relation to Y or F306. This means that the changes in the ΔG energy value were due to other pocket structural-chemical factors not governed by the Y306 residue. Because it is known that proteins are dynamic, the domain movements were detected using docking studies that showed various conformations and consequently, different ΔG values [44]. The ΔG value differences observed at the CS could be due to the CS entrance diameter (5 Å) as was observed in the native 3-D structures (1T67, 1T69, 1VKG and 2V5X) or in the other 3-D structures used (6 Å). This explains the lower affinity of VPA toward 1T67, 1T69, 1VKG, and 2V5X, shown in Table 1. This implied that the missing residues affected the ligand recognition of the 3-D HDAC structures. Approximately 13 residues were added to replace the missing residues in the middle of the protein for structures 1T67, 3EZP, 3EZT, 1T69, 1KKG, 1W22, 3F06, 3EW8 and 3F0R. The structural additions changed the VPA recognitions to

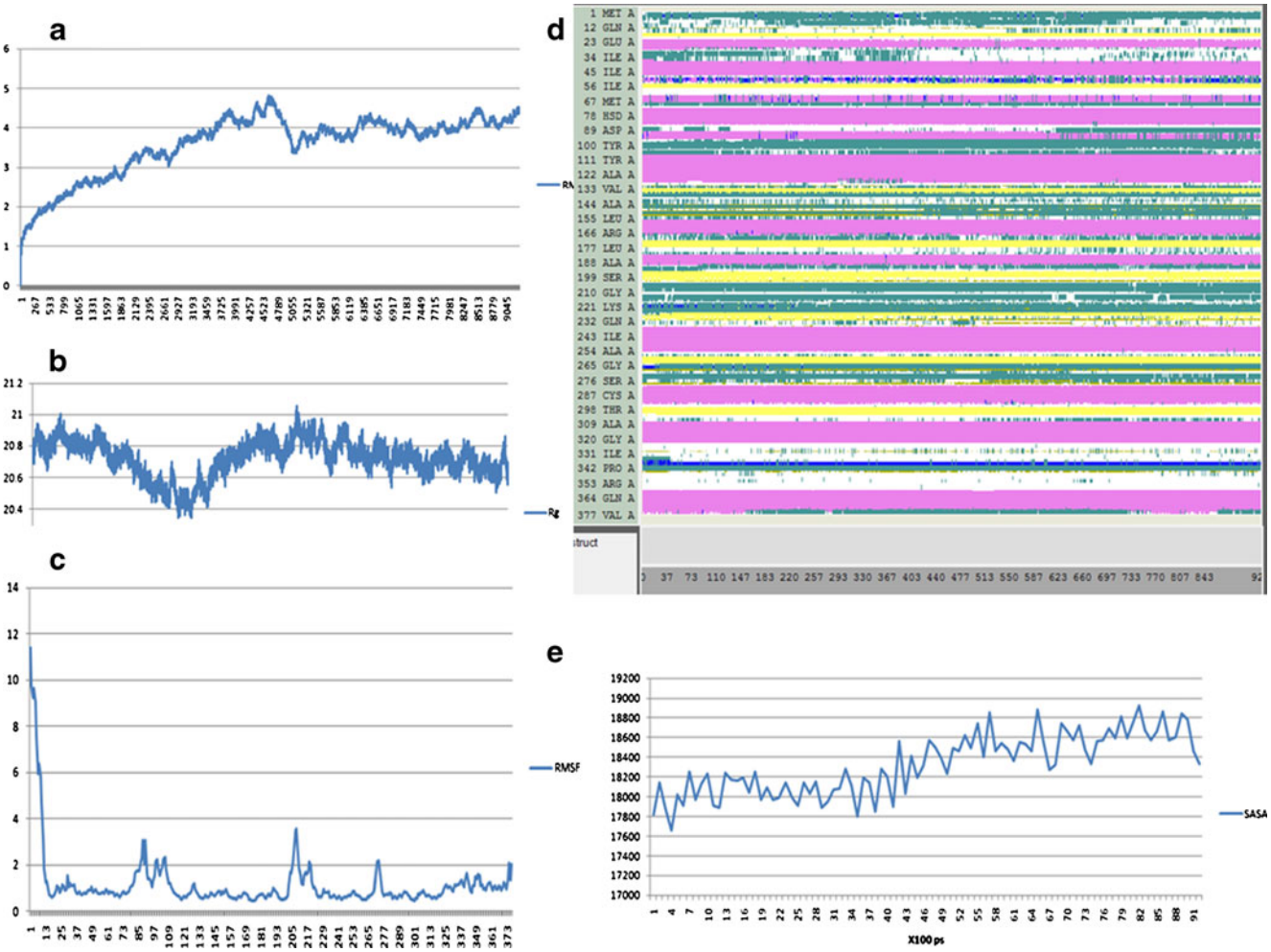

Fig. 3 (**a**) RMSD plots of the 9.5 ns MD simulations. (**b**) Rg values reaching protein stabilization. (**c**) RMSF values showing greater movements in the loops. (**d**) Secondary structure, which maintained its HDAC structures. (**e**) SASA values showing that the solvate protein surface was maintained after 5 ns

the CS and the HASC, as depicted in Table 1. Despite these structural modifications to the native 3-D structures, the highest affinity for VPA remained the HASC. Subsequently, the protein was minimized and then used for docking to allow the HDAC 3-D structural receptor to reach its optimal energy conditions [45]. The docking results showed that VPA had a lower affinity to HDAC in both sites than in the native 3-D structures, measuring between 0.1 - 0.5 mM for the CS and 0.01 - 0.05 mM for HASC. Despite all of the 3-D rebuilds and structural minimizations, VPA still recognized the HASC with more affinity than the CS (see Table 1). In conclusion, these complex theoretical analyses showed that VPA bound to the HDAC HASC in all 3-D HDACs tested (native and structurally modified by rebuilding and minimizing). To provide evidence that the HASC recognizes VPA and that the HASC could feasibly be the binding site for VPA, we employed MD simulations to show additional binding pockets [46] because of the many protein movements that docking scarcely considers.

The sequence alignments (Fig. 1) allowed us to choose the PDB structure most frequently cited in the literature [47], possibly due to the fact that it has a better 3-D structural quality. Furthermore, to demonstrate that the HASC was identified, we applied MD simulations, employing protocols used by our group, to allow for the treatment of macromolecules under physiological conditions, such as solvation, ions and protein flexibility [44, 48]. This is possible by combining docking and MD simulations [44, 48]. The MD simulation results demonstrated that in the first 4 ns, the HDAC structure was stable according to the RMSD, because 5 ns maintained the stability, until the simulation was finished (Fig. 3a). This was because the radius gyration decreased at 3 ns (Fig. 3b), but then it reached its initial value and maintained it with few changes. Similarly, the root mean square fluctuations (RMSF) were greater in residues 85–109, 205–217 and 277, as these residues belonged to well-known, identified HDAC8 loops [21]. As seen in Fig. 3c, greater movements were found in loop 202–212, which, together with loop 31–36, are near the CS where other ligands, such as *triconstatin* (TSA), bind. Greater loop movements were not influenced by the ligand recognition at the CS or HASC. It is important to mention that there are residues missing in some of the HDAC 3-D structures because they belong to the loop, and consequently, they show greater structural dynamics compared to those that form the CS and HASC. Figure 3d illustrates how the secondary structure was conserved, which suggests that the HDAC maintains its conformational behavior without risking protein deformity.

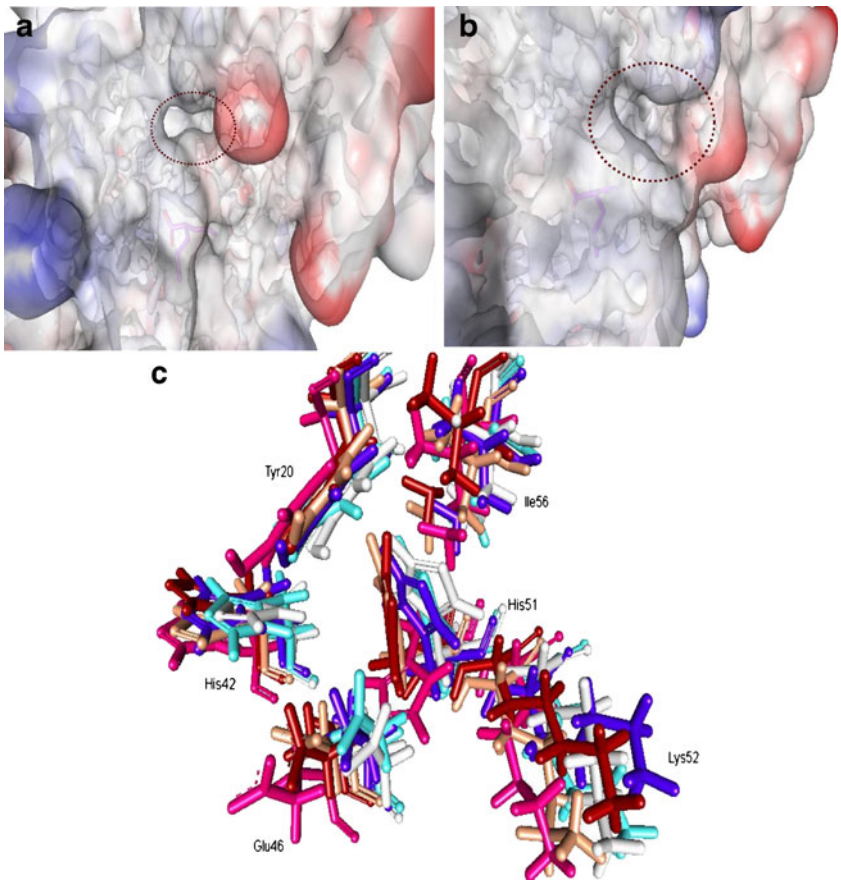

Fig. 4 Dynamics of the back door of the acetate release channel. (**a**) The door at the beginning of the MD simulations. (**b**) The door increases its diameter. (**c**) HASC residues and their movement during MD simulations

Last, the solvent accessible surface areas (SASA) initially increased, but after 5 ns, they remained constant. Furthermore, after this HDAC protein was validated, several snapshots (each 0.5 ns) from the 9.0 ns MD simulation were extracted to carefully explore the docking procedure for VPA binding to HDAC, as has been reported for other proteins. During the MD simulations, it was shown that the acetate release channel exhibited the same behavior, as was reported by Wang [43]. The reported conformational changes on the surface of the enzyme, particularly in the exit of the internal cavity of approximately 14 Å, were in accord with this result (Fig. 4a and b). This channel is connected to the CS and was conserved, as was illustrated using the MD simulations. These conformational changes were controlled primarily by I56, H51, H42 and E46. These residues appeared to act as a doorframe that was partially closed, but it then expanded during the first 4 ns (Fig. 4).

All of the conformational snapshots were screened against VPA by docking simulations, and the Kd remained predominantly around 0.5 mM. Short moments of low (1 mM) and high (0.05 mM) affinity were also observed. The reported Km for HDAC8 to deacylated ε-acylated lysyl moieties in histones is 0.03 mM [49]. While the experimental Ki of VPA to HDAC8 has not been reported, it was 0.4 mM in HDAC1 [9]. Taking this into account, VPA could be displaced from the catalytic site by the natural substrate, acetylated lysines, due to the higher affinity HDAC has toward them. However, it is possible that VPA inhibits HDAC function by blocking the back door escape of acetate, according to a previous study on structures taken from the PDB database. VPA interacted with the HASC in all snapshots. This confirmed that there was another site because VPA binds to the catalytic site; however, this does not entirely explain VPA's inhibitory effects. The greater affinity of VPA for the HASC (Table 1) was due to the several van der Waals interactions it has with Y18, I19, Y20, Y24, V25, R37, A38, V41, H42, I135, N136 and W137 as well as the hydrogen bonds it forms with S138 and I19.

The sequence of the catalytic site is conserved in class 1 HDACs; therefore, the Km value obtained for one isoform can be used for all. In this study, we obtained a Km similar to one determined empirically [9].

In conclusion, VPA binds with the CS by electrostatic interactions between the carboxyl group and the Zn atom, while VPA's hydrophobic chains are located at the base of the catalytic gorge without any evidence of hydrophobic interaction to explain VPA's low affinity (mM range). The docking procedures employing the crystal structures and MD simulations showed that VPA was located at the HASC, which blocks the release of the acetate and inhibits the HDAC catalytic activity. With these insights, new drug discovery strategies could now focus on designing compounds that target both the CS and the HASC, allowing selectivity for HDAC8.

Acknowledgments This study was conducted thanks to grants from Consejo Nacional de Ciencia y Tecnología, (132353), Instituto de Ciencia y Tecnología del Distrito Federal-Mexico, (PIRIVE09-9), Miguel Aleman A.C Foundation, and Secretaria de Investigación y Posgrado: Estimulo de desempeño en Investigación, Projects: 20110786 and Megaproyecto, Sistema de Becas por Exclusividad de Comisión de Cooperación y Fomento de Actividades Académicas del Instituto Politécnico Nacional. We also gratefully acknowledge the scholarships from Programa Institucional de Formación de Investigadores and from Consejo Nacional de Ciencia y Tecnología to JABL.

References

1. Marks PA, Jiang X (2005) Histone deacetylase inhibitors in programmed cell death and cancer therapy. Cell Cycle 4:549–551
2. Demonté D, Quivy V, Colette Y, van Lint C (2004) Administration of HDAC inhibitors to reactivate HIV-1 expression in latent cellular reservoirs: implications for the development of therapeutic strategies. Biochem Pharmacol 68:1231–1238
3. de Ruijter AJ, van Gennip AH, Caron HN, Kemp S, van Kuilenburg AB (2003) Histone deacetylases (HDACs): characterization of the classical HDAC family. Biochem J 370:737–749
4. Baylin SB, Esteller M, Rountree MR, Bachman KE, Schuebel K, Herman JG (2001) Aberrant patterns of DNA methylation, chromatin formation and gene expression in cancer. Hum Mol Genet 10:687–692
5. Hoshikawa Y, Kwon HJ, Yoshida M, Horinouchi S, Beppu T (1994) Trichostatin A induces morphological changes and gelsolin expression by inhibiting histone deacetylase in human carcinoma cell lines. Exp Cell Res 214:189–197
6. Yoshida M, Nomura S, Beppu T (1987) Effects of trichostatins on differentiation of murine erythroleukemia cells. Cancer Res 47:3688–3691
7. Medina V, Edmonds B, Young GP, James R, Appleton S, Zalewski PD (1997) Induction of caspase-3 protease activity and apoptosis by butyrate and trichostatin A (inhibitors of histone deacetylase): dependence on protein synthesis and synergy with a mitochondrial/cytochrome c–dependent pathway. Cancer Res 57:3697–3707
8. Bolden JE, Peart MJ, Johnstone RW (2006) Anticancer activities of histone deacetylase inhibitors. Nat Rev Drug Discov 5:769–784
9. Phiel CJ, Zhang F, Huang EY (2001) Histone deacetylase is a direct target of valproic acid, a potent anticonvulsant, mood stabilizer, and teratogen. J Biol Chem 276:36734–36741
10. Gurvich N, Tsygankova OM, Meinkoth JL, Klein PS (2004) Histone deacetylase is a target of valproic acid–mediated cellular differentiation. Cancer Res 64:1079–1086
11. Xia Q, Sung J, Chowdhury W, Chen CL, Hoti N, Shabbeer S, Carducci M, Rodriguez R (2006) Chronic administration of valproic acid inhibits prostate cancer cell growth in vitro and in vivo. Cancer Res 66:7237–7244
12. Kim TY, Bang YJ, Robertson KD (2006) Histone deacetylase inhibitors for cancer therapy. Epigenetics 1:14–23
13. Sharma S, Symanowski J, Wong B, Dino P, Manno P, Vogelzang N (2008) A phase II clinical trial of oral valproic acid in patients with castration-resistant prostate cancers using an intensive biomarker sampling strategy. Transl Oncol 1:141–147
14. MdeL M-G, Duenas-González A, Hernández-Montes J, De la Cruz-Hernández E, Pérez-Cárdenas E, Weiss-Steider B, Santiago-Osorio E, Ortíz-Navarrete VF, Rosales VH, Cantú D, Lizano-Soberón M, Rojo-Aguilar MP, Monroy-García A

(2006) Up-regulation of HLA class-I antigen expression and antigen-specific CTL response in cervical cancer cells by the demethylating agent hydralazine and the histone deacetylase inhibitor valproic acid. J Transl Med 4:55
15. Chavez-Blanco A, Perez-Plasencia C, Perez-Cardenas E, Carrasco-Legleu C, Rangel-Lopez E, Segura-Pacheco B, Taja-Chayeb L, Trejo-Becerril C, Gonzalez-Fierro A, Candelaria M, Cabrera G, Duenas-Gonzalez A (2006) Antineoplastic effects of the DNA methylation inhibitor hydralazine and the histone deacetylase inhibitor valproic acid in cancer cell lines. Cancer Cell Int 6:2
16. Abou-Zeid LA, El-Mowafy AM, Eikel D, Nau H, El-Mazar M (2007) Computational characteristics of valproic acid binding to histone deacetylase. Saudi Pharmaceutical J 15:3–4
17. C-Basurto J, Aburto J, T-Ferrara J, Torres E (2007) Ligand recognition by chloroperoxidase using molecular interaction fields and quantum chemestry claculations. Mol Simul 33:649–654
18. Espinoza-Fonseca LM, Trujillo-Ferrara JC (2006) The existence of a second allosteric site on the M1 muscarinic acetylcholine receptor and its implications for drug design. Bioorg Med Lett 16:1217–1220
19. Aburto J, Correa-Basurto J, Torres E (2008) Atypical kinetic behavior of chloroperoxidase-mediated oxidative halogenation of polycyclic aromatic hydrocarbons. Arch Biochem Biophys 480:33–40
20. Somoza JR, Skene RJ, Katz BA, Mol C, Ho JD, Jennings AJ, Luong C, Arvai A, Buggy JJ, Chi E, Tang J, Sang BC, Verner E, Wynands R, Leahy EM, Dougan DR, Snell G, Navre M, Knuth MW, Swanson RV, McRee DE, Tari LW (2004) Structural snapshots of human HDAC8 provide insights into the class I histone deacetylases. Structure 12:1325–1334
21. Vannini A, Volpari C, Filocamo G, Caroli Casavola E, Brunetti M, Renzoni D, Chakravarty P, Paolini C, De Francesco R, Gallinari P, Steinckuhler C, Di Marco S (2004) Crystal structure of a eukaryotic Zn-dependent histone deacetylase, human Hdac8, complexed with a hydroxamic acid inhibitor. PNAS 101:15064–15069
22. Vannini A, Volpari C, Gallinari P, Jones P, Mattu M, Carfí A, De Francesco R, Steinkühler C, Di Marco S (2007) Substrate binding to histone deacetylases as shown by the crystal structure of the HDAC8-substrate complex. EMBO Rep 8:879–884
23. Dowling DP, Gantt SL, Gattis SG, Fierke CA, Christianson DW (2008) Structural studies of human histone deacetylase 8 and its site-specific variants complexed with substrate and inhibitors. Biochemistry 47:13554–13563
24. Larkin MA, Blackshields G, Brown NP, Chenna R, McGettigan PA, McWilliam H, Valentin F, Wallace IM, Wilm A, Lopez R, Thompson JD, Gibson TJ, Higgins DG (2007) Clustal W and clusta X version 2.0. Bioinformatics 23:2947–2948
25. Waterhouse AM, Procter JB, Martin DM, Clamp M, Barton GJ (2009) Jalview Version 2–a multiple sequence alignment editor and analysis workbench. Bioinformatics 25:1189–1191
26. Sali A, Blundell TL (1993) Comparative protein modelling by satisfaction of spatial restraints. J Mol Biol 234:779–815
27. ISIS/Draw, MDL Information System, 14600 Catalina Street, San Leandro, CA 94677, USA. The program (editions of 2.5 and 2.3) is available at the MDL at http://www.mdii.com
28. WebLab Viewer, available at http://www.liv.ac.uk/ctichem/16weblab.html
29. Frisch MJ, Trucks GW, Schlegel HB, Scuseria GE, Robb MA, Cheeseman JR, Zakrzewski VG, Montgomery JA, Stratmannm RE, Burant JC, Dapprich S, Millam JM, Daniels AD, Kudin KN, Strain MC, Farkas O, Tomasi J, Barone V, Cossi M, Cammi R, Mennucci B, Pomelli C, Adamo C, Clifford S, Ochterski J, Peterson GA, Ayala PY, Cui Q, Morokuma K, Malick DK, Rabuck AD, Raghavachari K, Foresman JB, Cioslowski J, Ortiz JV, Baboul AG, Stefanov BB, Liu G, Liashenko A, Piskorz P, Komaromi I, Gomperts R, Martin RL, Fox DJ, Keith T, Al-Laham MA, Peng CY, Nanayakkara A, Challacombe M, Gill PMW, Johnson B, Chen W, Wong MW, Andres JL, Gonzalez C, Head-Gordon M, Replogle ES, Pople JA (1998) Gaussian 98, Revision A.9. Gaussian Inc, Pittsburgh
30. Morris GM, Goodsell DS, Halliday RS, Huey R, Hart WE, Belew RK, Olson AJ (1998) Automated docking using a Lamarckian genetic algorithm and an empirical binding free energy function. J Comput Chem 19:1639–1662
31. Phillips C, Braun R, Wang W, Gumbart J, Tajkhorshid E, Villa E, Chipot C, Skeel RD, Kale L, Schulten K (2005) Scalable molecular dynamics with NAMD. J Comput Chem 26:1781–1802
32. MacKerell AD Jr, Bashford D, Bellott M, Dunbrack RL Jr, Evanseck J, Field MJ, Fischer S, Gao J, Guo H, Ha S, Joseph D, Kuchnir L, Kuczera K, Lau FTK, Mattos C, Michnick S, Ngo T, Nguyen DT, Prodhom B, Reiher IWE, Roux B, Schlenkrich M, Smith J, Stote R, Straub J, Watanabe M, Wiorkiewicz-Kuczera J, Yin D, Karplus M (1998) All-atom empirical potential for molecular modeling and dynamics studies of proteins. J Phys Chem B 102:3586–3616
33. Humphrey W, Dalke A, Schulten K (1996) VMD: visual molecular dynamics. J Mol Graph 14:33–38
34. Batcho PF, Case DA, Schlick T (2001) Optimized particle-mesh Ewald/multiple-timestep integration for molecular dynamics simulation. J Chem Phys 115:4003–4041
35. Martyna GJ, Tobias DJ, Klein ML (1994) Constant-pressure molecular-dynamics algorithms. J Chem Phys 101:4177–4189
36. Ryckaert JP, Ciccotti G, Berendsen HJC (1977) Numerical integration of the cartesian equations of motion of a system with constrains. J Comput Phys 23:327–341
37. Glykos NM (2006) Carma: a molecular dynamics analysis program. J Comput Chem 27:1765–1768
38. Bieliauskas AV, Pflum MK (2008) Isoform-selective histone deacetylase inhibitors. Chem Soc Rev 37:1402–1413
39. Khan N, Jeffers M, Kumar S, Hacket C, Boldog F, Khramtsov N, Qian X, Mills E, Berghs SC, Carey N, Finn PW, Collins LS, Tumber A, Ritchie JW, Jensen PB, Lichenstein HS, Sehested M (2008) Determination of the class and isoform selectivity os small-molecule histone deacetylase inhibitors. Biochem J 409:581–589
40. Mai A, Massa S, Pezzi R, Rotili D, Loidl P, Brosch G (2003) Discovery of (aryloxopropenyl)pyrrolyl hydroxyamides as selective inhibitors of class IIa histone deacetylase homologue HD1-A. J Med Chem 46:4826–4829
41. Perez-Balado C, Nebbioso A, Rodriguez-Grana P, Minichiello A, Miceli M, Altucci L, de Lera AR (2007) Bispyridinium dienes: histone deacetylase inhibitors with selective activities. J Med Chem 50:2497–2505
42. Ogiso T, Ito Y, Iwaki M, Yamamoto Y, Yamahata T (1987) Percutaneous absorption of valproic acid and its plasma concentration after application of ointment. J Pharmacobiodyn 10:537–542
43. Wang DF, Wiest O, Helquist P, Lan-Hargest HY, Wiech NL (2004) On the function of the 14 Å long internal cavity of histone deacetylase-like protein: implications for the design of histone deacetylase inhibitors. J Med Chem 47:3409–3417
44. Deeb O, Rosales-Hernández MC, Gómez-Castro C, Garduño-Juárez R, Correa-Basurto J (2010) Exploration of human serum albumin binding sites by docking and molecular dynamics flexible ligand-protein interactions. Biopolymers 93:161–170
45. Soriano-Ursúa MA, Trujillo-Ferrara JG, Correa-Basurto J (2009) Homology modeling and flex-ligand docking studies on the guinea pig beta(2) adrenoceptor: structural and experimental

similarities/ differences with the human beta(2). J Mol Model 15:1203–1211
46. Ozbabacan SE, Gursoy A, Keskin O, Nussinov R (2010) Conformational ensembles, signal transduction and residue hot spots: application to drug discovery. Curr Opin Drug Discov Devel 13:527–537
47. Estiu G, West N, Mazitschek R, Greenberg E, Bradner JE, Wiest O (2010) On the inhibition of histone deacetylase 8. Bioorg Med Chem 18:4103–4110
48. Rosales-Hernández MC, Mendieta-Wejebe JE, Trujillo-Ferrara JG, Correa-Basurto J (2010) Homology modeling and molecular dynamics of CYP1A1 and CYP2B1 to explore the metabolism of aryl derivatives by docking and experimental assays. Eur J Med Chem 45:4845–4855
49. Riester D, Hildmann C, Grünewald S, Beckers T, Schwienhorst A (2007) Factors affecting the substrate specificity of histone deacetylases. Biochem Biophys Res Commun 357:439–445